JOURNAL OF GUIDANCE, CONTROL, AND DYNAMICS
Vol. 31, No. 5, September–October 2008

Linear Quadratic Guidance Laws for Imposing a Terminal Intercept Angle

Vitaly Shaferman* and Tal Shima†
Technion–Israel Institute of Technology, 32000 Haifa, Israel

DOI: 10.2514/1.32836

Linear quadratic guidance laws that explicitly enable imposing a predetermined intercept angle are presented. Two such guidance laws are derived, using optimal control and differential game theories, for arbitrary-order linear missile dynamics. The obtained guidance laws are dependent on the well-known zero-effort miss distance and on a new variable denoted zero-effort angle. It is shown that imposing the terminal angle constraint raises considerably the gains of the guidance laws. Theoretic conditions for the existence of a saddle-point solution in the differential game are also derived. These conditions show that imposing the terminal angle constraint requires a higher maneuverability advantage from the missile. The performance of the proposed guidance laws is investigated using a nonlinear two-dimensional simulation of the missile's lateral dynamics and relative kinematics, while assuming first-order dynamics for the target's evasive maneuvers. Using a Monte Carlo study, it is shown that, for the investigated problem, a target can be intercepted with a negligible miss distance and intercept angle error even when the target maneuvers and there are large initial heading errors.

I. Introduction

THE angle at which a target is intercepted is an important parameter in a missile guidance problem, as it affects warhead lethality and the target's capability to effectively employ countermeasures. Using traditional guidance laws, such as proportional navigation (PN), the interception angle cannot be imposed. It is mainly a function of the initial collision triangle and the target maneuver.

Previous works on intercept angle control mainly include optimal guidance laws (OGLs) and modified PN-type laws. In [1], an optimal control law for intercept angle error and miss distance minimization was proposed for a reentry vehicle pursuing a fixed or slowly moving ground target. The guidance law was formulated in a missile fixed Cartesian coordinate system and minimized a quadratic cost function. In [2,3], optimal control laws, for a missile with arbitrary-order dynamics trying to hit a stationary target, were proposed with a similar cost function and a line-of-sight (LOS) fixed coordinate system. The proposed law was implemented for lag-free and first-order lag missile systems. Ryoo et al. [4] used the same formulation as in [2,3], but extended the previous works by adopting a time-to-go weighted energy cost function to shape the missile's trajectory. One of the underlying assumptions in all of these works is a stationary or slowly moving target.

In [5], an optimal guidance law for intercept angle control of a maneuvering ship and a missile with varying velocity was proposed. The guidance law was formulated in a Cartesian coordinate system with one axis pointing toward the required missile terminal heading. The authors assumed a constant, and relatively low, target maneuver and a small initial heading error. The resulting guidance law required extensive information, including the perpendicular position and speed relative to the terminal heading, and the target's path angle and angular rate. To fulfill these requirements, a suboptimal estimation filter was integrated in the proposed solution. Kim et al. [6] presented a biased PN law for an impact with a predefined missile attitude angle against a moving target. A time-varying component was added to the LOS rate of the PN guidance law. For the derivation, linearization and time-to-go estimation were not required. It was shown through simulation that the guidance law provides acceptable performance against slowly maneuvering targets. In [7], optimal control planar interception laws against maneuvering targets with known trajectories were presented. The authors derived guidance laws for a lag-free missile with constraints on the initial and final flight-path angles of the interceptor and a cost on the flight time and control effort of the missile. The solution requires numerically finding four constants and the number of interceptor acceleration sign switches along the trajectory.

In [8], a simple rendezvous of an interceptor and a nonmaneuvering target was solved. The formulation included quadratic penalties on the terminal relative displacement and relative terminal velocity to the required rendezvous course. This formulation can be used to impose a terminal intercept angle in such a scenario by selecting the ratio between the relative terminal velocity and the closing speed. In [9], a similar formulation was used to derive linear quadratic OGLs and linear quadratic differential game (LQDG) based laws for maneuvering target scenarios. The guidance laws were derived using a linearization around the collision course. This formulation does not enable direct intercept angle control. However, for the OGL case, a required intercept angle can be reformulated to a required relative velocity, resulting in an indirect intercept angle control.

In this paper, we propose OGL and LQDG-type guidance laws, for arbitrary-order linear missile dynamics, which explicitly enable imposing a predetermined intercept angle. Because of the complexity of the derivation, analytic terms are derived only for the ideal missile dynamics case. The remainder of this paper is organized as follows: In the next section, the mathematical models used for the guidance laws' derivation and simulation are presented. A constrained terminal intercept angle optimal guidance law (OGL-CTIA) is derived in Sec. III. In Sec. IV, a constrained terminal intercept angle linear quadratic differential game law (LQDG-CTIA) is derived. A performance analysis is presented in Sec. V, followed by concluding remarks. In the Appendix, an equivalent derivation of the guidance laws is provided.

II. Models Derivation

A skid-to-turn roll-stabilized missile is considered. The motion of such a missile can be separated into two perpendicular channels. In Fig. 1, a schematic view of the planar endgame geometry is shown,

Received 15 June 2007; revision received 31 March 2008; accepted for publication 8 April 2008.

*Graduate Student, Department of Aerospace Engineering; vitalysh@tx.technion.ac.il.

†Senior Lecturer, Department of Aerospace Engineering; tal.shima@technion.ac.il. Senior Member AIAA.

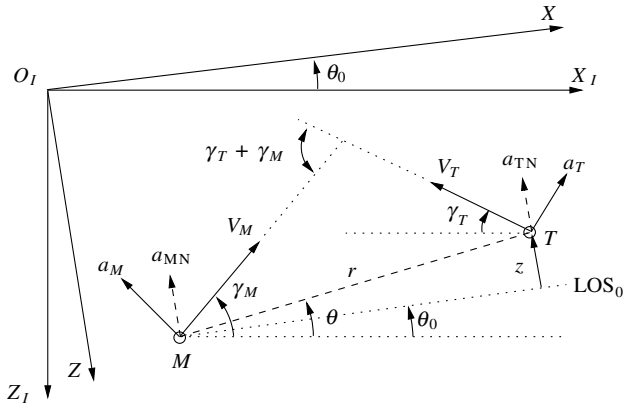

Fig. 1 Planar engagement geometry.

where $X_I - O_I - Z_I$ is a Cartesian inertial reference frame. We denote the missile and target by the subscripts M and T, respectively. The speed, normal acceleration, and flight-path angles are denoted by V, a, and γ, respectively; the range between the adversaries is r, and θ is the angle between the LOS and the X_I axis. The X axis, aligned with the LOS used for linearization, is denoted as LOS_0. The relative displacement between the target and the missile normal to this direction is z. The target and missile accelerations normal to LOS_0 are denoted by a_{TN} and a_{MN}, respectively, and satisfy $a_{TN} = a_T \cos(\gamma_{T0} + \theta_0)$, $a_{MN} = a_M \cos(\gamma_{M0} - \theta_0)$. We denote the required intercept angle $(\gamma_T + \gamma_M)$ as x_4^c.

Next, we present the full nonlinear kinematics equations of the interception problem, which will be used in the nonlinear simulation in Sec. V. Then, the linearized equations, which will be used to derive the proposed guidance laws, will be presented.

A. Nonlinear Kinematics

Neglecting the gravitational force, the engagement kinematics, expressed in a polar coordinate system (r, θ) attached to the missile, are

$$\dot{r} = V_r \tag{1a}$$

$$\dot{\theta} = V_\theta / r \tag{1b}$$

where the speed V_r is

$$V_r = -[V_M \cos(\gamma_M - \theta) + V_T \cos(\gamma_T + \theta)] \tag{2}$$

and the speed perpendicular to the LOS is

$$V_\theta = -V_M \sin(\gamma_M - \theta) + V_T \sin(\gamma_T + \theta) \tag{3}$$

During the endgame, the target and missile are assumed to move at a constant speed. In addition, we assume first-order lateral maneuver dynamics for the target

$$\dot{a}_T = (w_T - a_T)/\tau_T \tag{4a}$$

$$\dot{\gamma}_T = a_T / V_T \tag{4b}$$

where τ_T is the time constant of the target dynamics and w_T is the target's acceleration command.

In endoatmospheric interception, the majority of the interceptor's lift is usually obtained by generating an angle of attack; a process that has dynamics. The interceptor has steering devices, such as canard or tail, that can generate angle of attack, and, neglecting servo dynamics, possibly instantaneous maneuvers. We assume that the dynamics during the endgame can be represented by arbitrary-order linear equations

$$\dot{\mathbf{x}}_M = \mathbf{A}_M \mathbf{x}_M + \mathbf{B}_M u_M \tag{5a}$$

$$\dot{\gamma}_M = a_M / V_M \tag{5b}$$

where

$$a_M = \mathbf{C}_M \mathbf{x}_M + d_M u_M \tag{6}$$

and $\mathbf{x}_M$ is the state vector of the interceptor's internal state variables with $\dim(\mathbf{x}_M) = n$. We denote the part of the acceleration without dynamics, if it exists, as the direct lift, whereas the part with dynamics is referred to as the specific force. These equations can represent the closed-loop missile dynamics. They can also represent the linearized open-loop dynamics, in which case the obtained guidance law will actually be an integrated guidance-autopilot controller [10].

B. Linearized Kinematics for Guidance Law Derivation

The derivation of the guidance laws in this paper will be performed based on a linearized model. If, during the endgame, the missile and target deviations from the collision triangle are small, that is, the endgame is initiated with a collision triangle satisfying closely the requirement on the intercept angle $x_4^c = \gamma_M + \gamma_T$, and the target's maneuver relative to its speed is small, then the linearization is justified. This initialization can be performed, for example, by a nonlinear midcourse guidance law. If, on the other hand, the scenario is not initiated on the required collision triangle (as in some of the cases simulated in Sec. V) and/or the target has a large maneuver capability relative to its speed, then we resort to extended linearization or state-dependent Riccati-equation-like techniques [11]. We will linearize the equations of motion at each step of time and then solve the associated state-dependent Riccati equation. To obtain an implementable scheme, we will seek an analytic solution for this equation, thus not requiring the online solution of the Riccati equation at each time step.

The state vector of the linearized problem is

$$\mathbf{x} = [z \quad \dot{z} \quad a_T \quad (\gamma_T + \gamma_M) \quad \mathbf{x}_M^T]^T \tag{7}$$

The equations of motion are

$$\dot{\mathbf{x}} = \begin{cases} \dot{x}_1 = x_2 \\ \dot{x}_2 = a_T \cos(\gamma_{T0} + \theta_0) - a_M \cos(\gamma_{M0} - \theta_0) \\ \dot{x}_3 = (w_T - a_T)/\tau_T \\ \dot{x}_4 = a_T / V_T + a_M / V_M \\ \dot{\mathbf{x}}_M = \mathbf{A}_M \mathbf{x}_M + \mathbf{B}_M u_M \end{cases} \tag{8}$$

The matrix form of the equation set is therefore

$$\dot{\mathbf{x}} = \mathbf{A}\mathbf{x} + \mathbf{B}u_M + \mathbf{C}w_T \tag{9}$$

where

$$\mathbf{A} = \begin{bmatrix} \mathbf{A}_k & \mathbf{A}_{12} \\ [0]_{n\times 4} & \mathbf{A}_M \end{bmatrix}, \quad \mathbf{B} = \begin{bmatrix} 0 \\ -d_M \cos(\gamma_{M0} - \theta_0) \\ 0 \\ d_M / V_M \\ \mathbf{B}_M \end{bmatrix}, \quad \mathbf{C} = \begin{bmatrix} 0 \\ 0 \\ 1/\tau_T \\ 0 \\ [0]_{n\times 1} \end{bmatrix} \tag{10}$$

and

$$\mathbf{A}_k = \begin{bmatrix} 0 & 1 & 0 & 0 \\ 0 & 0 & \cos(\gamma_{T0} + \theta_0) & 0 \\ 0 & 0 & -1/\tau_T & 0 \\ 0 & 0 & 1/V_T & 0 \end{bmatrix}, \quad \mathbf{A}_{12} = \begin{bmatrix} [0]_{1\times n} \\ -\mathbf{C}_M \cos(\gamma_{M0} - \theta_0) \\ [0]_{1\times n} \\ \mathbf{C}_M / V_M \end{bmatrix} \tag{11}$$

with [0] denoting a matrix of zeros with appropriate dimensions.

Once a collision triangle is reached and maintained, the speed V_r is constant and the interception time, given by $t_f = -r_0/V_r$, can be assumed fixed. For the guidance law implementation, we approximate time to go by

$$t_{\text{go}} = -r/V_r \tag{12}$$

III. Optimal Guidance Law

In this section, we are solving a one-sided optimization problem. We assume knowledge of the future maneuver strategy of the target and that it is to maintain a constant maneuver. Thus, $w_T = a_T$ during the engagement scenario.

The quadratic cost function chosen for the OGL was

$$J = \frac{a}{2}x_1^2(t_f) + \frac{b}{2}[x_4(t_f) - x_4^c]^2 + \frac{1}{2}\int_0^{t_f} u^2\,\mathrm{d}t \tag{13}$$

where the weights a, b are nonnegative. The projection of the interceptor's command in the direction perpendicular to LOS_0 is $u = u_M\cos(\gamma_{M0} - \theta_0)$, and we assume that, during the endgame, $|\gamma_{M0} - \theta_0| < \pi/2$. Note that letting $a \to \infty$ yields a perfect intercept guidance law, and letting $b \to \infty$ results in a perfect intercept angle guidance law.

Remark: An integral cost on u^2 is a common representation of the interceptor's control effort [9,12]. It also enables comparing, in the limiting cases, the results obtained in this paper to previously published ones. When $|\gamma_{M0} - \theta_0|$, the angle between the missile's velocity vector and LOS_0, is close to $\pi/2$, an integral cost on u_M^2 may be more appropriate for the following reasons:

1) It enables a more straightforward tradeoff between the running cost and the terminal one.

2) If the interception geometry changes throughout the engagement (requiring relinearization) then, to maintain this tradeoff, there is no need to tune the weights.

3) Such a formulation ensures that the gains and the control command u_M do not diverge when $\cos(\gamma_{M0} - \theta_0)$ approaches zero. Therefore, in the Appendix, an equivalent representation, but with a running cost on u_M^2, is also provided.

A. Order Reduction

Bryson and Ho [8] introduced a transformation enabling reducing a problem's order. This transformation is sometimes denoted as terminal projection. We will use a similar transformation.

Let us define a new state vector $\mathbf{Z}(t)$ that satisfies

$$\mathbf{Z}(t) = \mathbf{D}\boldsymbol{\Phi}(t_f, t)\mathbf{x}(t) + \mathbf{D}\int_t^{t_f} \boldsymbol{\Phi}(t_f, \tau)\mathbf{C}a_T\,\mathrm{d}\tau \tag{14}$$

where $\boldsymbol{\Phi}(t_f, t)$ is the transition matrix associated with Eq. (9), and $\mathbf{D}$ is a constant matrix

$$\mathbf{D} = \begin{bmatrix} 1 & 0 & 0 & 0 & [0]_{1\times n} \\ 0 & 0 & 0 & 1 & [0]_{1\times n} \end{bmatrix} \tag{15}$$

Then, the derivative with respect to time of the new state vector $\mathbf{Z}(t)$ is

$$\dot{\mathbf{Z}} = \mathbf{D}[\dot{\boldsymbol{\Phi}}(t_f, t)\mathbf{x} + \boldsymbol{\Phi}(t_f, t)\dot{\mathbf{x}}] - \mathbf{D}\boldsymbol{\Phi}(t_f, t)\mathbf{C}a_T = \mathbf{D}\boldsymbol{\Phi}(t_f, t)\mathbf{B}u_M \tag{16}$$

which is state independent. $\mathbf{Z}(t_f)$ can be expressed using Eq. (14) as

$$\mathbf{Z}(t_f) = \mathbf{D}\mathbf{x}(t_f) = \begin{bmatrix} x_1(t_f) \\ x_4(t_f) \end{bmatrix} \tag{17}$$

Using these new variables, the cost function from Eq. (13) can also be expressed using only the new state vector $\mathbf{Z}(t)$ as

$$J = \frac{a}{2}Z_1^2(t_f) + \frac{b}{2}[Z_2(t_f) - x_4^c]^2 + \frac{1}{2}\int_0^{t_f} u^2\,\mathrm{d}t \tag{18}$$

Note that, besides reducing the order of the problem, the two variables of the new state vector $\mathbf{Z}(t)$ have an important physical meaning. $Z_1(t)$ is known as the zero-effort miss (ZEM), which, in a one-sided optimization problem, is the miss distance if, from the current time onward, the missile will not apply any control and the target will perform its known maneuver (in our case, constant maneuver). We will refer to the new term $Z_2(t)$ as zero-effort angle (ZEA), which, in an analogy to the ZEM, is the intercept angle if, from the current time onward, the missile will not apply any control and the target will perform its known maneuver. We denote $[Z_2(t) - x_4^c]$ as the zero-effort angle error (ZEAE).

B. Optimal Controller

The Hamiltonian of the problem is

$$H = \frac{1}{2}u^2 + \dot{Z}_1\lambda_1 + \dot{Z}_2\lambda_2 \tag{19}$$

The adjoint equations and solutions are

$$\begin{cases} \dot{\lambda}_1 = -\frac{\partial H}{\partial Z_1} = 0; \quad \lambda_1(t_f) = aZ_1(t_f) \\ \dot{\lambda}_2 = -\frac{\partial H}{\partial Z_2} = 0; \quad \lambda_2(t_f) = b[Z_2(t_f) - x_4^c] \end{cases} \Rightarrow \begin{cases} \lambda_1(t) = aZ_1(t_f) \\ \lambda_2(t) = b[Z_2(t_f) - x_4^c] \end{cases} \tag{20}$$

The optimal controller for the missile satisfies $u^* = \arg_u \min H$.

For obtaining an analytic solution for the guidance law u^*, we will assume dealing with a missile having ideal dynamics, that is, zero lag. This simplifies the time derivatives of $\mathbf{Z}$ to

$$\begin{cases} \dot{Z}_1 = -(t_f - t)\cos(\gamma_{M0} - \theta_0)u_M \\ \dot{Z}_2 = u_M/V_M \end{cases} \Rightarrow \begin{cases} \dot{Z}_1 = -(t_f - t)u \\ \dot{Z}_2 = u/v'_M \end{cases} \tag{21}$$

where $v'_M = V_M\cos(\gamma_{M0} - \theta_0)$ is the missile's velocity component on LOS_0.

Remark: According to Eq. (21), when $\cos(\gamma_{M0} - \theta_0) \to 0$, the system is uncontrollable with respect to u_M. In such a case, the missile's velocity vector is perpendicular to the initial LOS and it does not have control authority in this direction. Note that a similar phenomenon appears in other linear guidance laws, such as the well-known augmented PN (APN) and OGL [12]. Using an integral cost on u_M, as in the Appendix, can ensure that the navigation gain, as well as the control u_M, are bounded for such a case.

For the considered ideal dynamics, the optimal guidance law simplifies to

$$\begin{aligned} \frac{\partial H}{\partial u} = 0 \Rightarrow u^*(t) &= \lambda_1(t_f - t) - \lambda_2/v'_M \\ &= aZ_1(t_f)(t_f - t) - \frac{b}{v'_M}[Z_2(t_f) - x_4^c] \end{aligned} \tag{22}$$

Substituting Eq. (22) into Eq. (21), and integrating from t to t_f, using the end conditions from Eq. (17) yields the following two coupled algebraic equations:

$$Z_1(t_f) = Z_1(t) - aZ_1(t_f)\frac{(t_f - t)^3}{3} + \frac{b}{v'_M}[Z_2(t_f) - x_4^c]\frac{(t_f - t)^2}{2} \tag{23a}$$

$$Z_2(t_f) = Z_2(t) + \frac{a}{v'_M}Z_1(t_f)\frac{(t_f - t)^2}{2} - \frac{b}{v'^2_M}[Z_2(t_f) - x_4^c](t_f - t) \tag{23b}$$

Solving for $Z_1(t_f)$ and $Z_2(t_f)$ and substituting the solution into Eq. (22) yields the following optimal controller:

$$u^*(t) = \frac{N_{\text{ZEM}}}{t_{\text{go}}^2}Z_1(t) + N_{\text{ZEAE}}\frac{v'_M}{t_{\text{go}}}[Z_2(t) - x_4^c] \tag{24}$$

where

$$Z_1(t) = z + \dot{z}t_{\text{go}} + a_T \cos(\gamma_{T0} + \theta_0)t_{\text{go}}^2/2 \tag{25a}$$

$$Z_2(t) = t_{\text{go}} a_T / V_T + \gamma_T + \gamma_M \tag{25b}$$

and

$$\begin{aligned} N_{\text{ZEM}} &= \frac{3at_{\text{go}}^3}{3 + at_{\text{go}}^3} + \frac{bK_3(t_{\text{go}})K_2(t_{\text{go}})t_{\text{go}}^2}{K_1(t_{\text{go}}) + v_M'^2}, \\ N_{\text{ZEAE}} &= \frac{bK_3(t_{\text{go}})t_{\text{go}}}{K_1(t_{\text{go}}) + v_M'^2} \end{aligned} \tag{26}$$

$$K_1(t_{\text{go}}) = \frac{b(at_{\text{go}}^4 + 12t_{\text{go}})}{4(3 + at_{\text{go}}^3)}, \qquad K_2(t_{\text{go}}) = \frac{3at_{\text{go}}^2}{2(3 + at_{\text{go}}^3)}$$

$$K_3(t_{\text{go}}) = \frac{at_{\text{go}}^3 - 6}{2(3 + at_{\text{go}}^3)} \tag{27}$$

The closed-loop form guidance law in Eq. (24) is linear with respect to both the ZEM and the ZEAE. N_{ZEM} and N_{ZEAE} are bounded for $0 < t_{\text{go}} \leq t_f$, regardless of the values of a, b, and v_M'. Therefore, u^* is bounded. A conjugate point does not exist if and only if the gains are bounded [9] for all $0 < t_{\text{go}} \leq t_f$, consequently, a conjugate point does not exist in this case.

The required information for the implementation of the guidance law is, therefore, $Z_1(t)$, $Z_2(t)$, t_{go}, and v_M'. By using the small deviation from the collision triangle assumption, the displacement z normal to the initial LOS can be approximated by

$$z \approx (\theta - \theta_0)r \tag{28}$$

Differentiating Eq. (28) with respect to time yields

$$z + \dot{z}t_{\text{go}} = -V_r t_{\text{go}}^2 \dot{\theta} \tag{29}$$

Using this expression, $Z_1(t)$ of Eq. (25a) can be expressed as

$$Z_1(t) = -V_r t_{\text{go}}^2 \dot{\theta} + a_T \cos(\gamma_{T0} + \theta_0)t_{\text{go}}^2/2 \tag{30}$$

By using a radar seeker and an inertial navigation system, v_M', V_r, and γ_M can be directly measured, whereas $\dot{\theta}$, γ_T, a_T, V_T, and the t_{go} must be estimated. Note that t_{go} can be estimated using Eq. (12), but a more accurate t_{go} estimation might be needed, such as the one presented in [3].

C. Navigation Gains

Let us now examine the values of the navigation gains of Eq. (26). By choosing $b \to 0$, we no longer impose an intercept angle, resulting in $N_{\text{ZEAE}} \to 0$, and the degeneration of the guidance law in Eq. (24) to the OGL presented in [9]. If we also choose $a \to \infty$, which dictates zero miss, the guidance law further degenerates to the well-known APN guidance law [13] with $N_{\text{ZEM}} = 3$.

For a perfect intercept with some account for terminal intercept angle, we would require $a \to \infty$ and finite b, resulting in the degeneration of the navigation gains in Eqs. (26) to

$$\begin{aligned} N_{\text{ZEM}}(a \to \infty) &= 3 + \frac{3bt_{\text{go}}}{bt_{\text{go}} + 4v_M'^2}, \\ N_{\text{ZEAE}}(a \to \infty) &= \frac{2bt_{\text{go}}}{bt_{\text{go}} + 4v_M'^2} \end{aligned} \tag{31}$$

Figure 2 presents the time history of the navigation gains for a perfect intercept ($a \to \infty$) and various values for b. Note that the navigation gains are constant with respect to t_{go} for $b \to 0$ and $b \to \infty$. The gains increase with t_{go} for $0 < b < \infty$ and for $t_{\text{go}} \to \infty$ they are not a function of b.

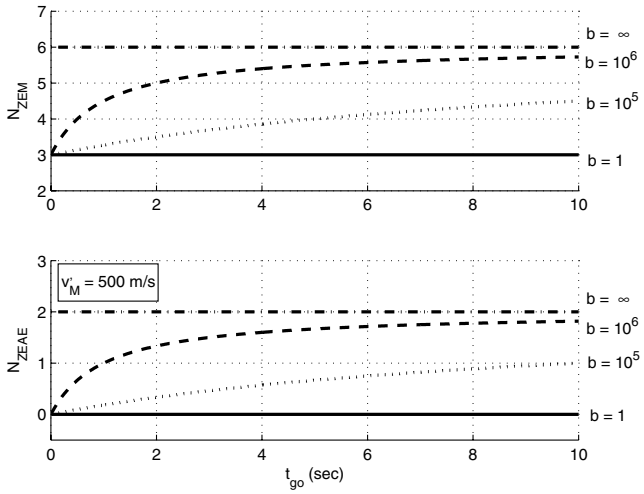

Fig. 2 Perfect intercept ($a \to \infty$) OGL-CTIA navigation gains.

For perfect intercept and for perfect intercept angle as well, we also need to dictate $b \to \infty$, for which the navigation gains degenerate to those of the simple rendezvous presented in [8]:

$$N_{\text{ZEM}}(a \to \infty, b \to \infty) = 6, \qquad N_{\text{ZEAE}}(a \to \infty, b \to \infty) = 2 \tag{32}$$

Note that, similar to the optimal APN and the PN cases, the navigation gains for the $b \to \infty$ case are not a function of time to go. Another interesting observation is that the gain associated with the ZEM is multiplied by a factor of 2 compared with the optimal PN and APN cases, which might result in an increased sensitivity to measurement noise.

D. Perfect Intercept and Perfect Intercept Angle

We now present the optimal trajectories resulting from using the proposed guidance law for the perfect intercept and intercept angle case.

The terminal projection transformation enabled us to reduce the optimization space to two dimensions, governed by Eq. (21). Let us now perform the following transformation:

$$\bar{\mathbf{Z}}(t) = \begin{bmatrix} Z_1(t) \\ Z_2(t) - x_4^c \end{bmatrix} \tag{33}$$

The new state vector $\bar{\mathbf{Z}}(t)$ uses the ZEAE as the second state instead of the ZEA, enabling us to present the optimal solutions in a more intuitive manner. In the new 3-D space (t_{go}, ZEM, ZEAE) perfect intercept should terminate in the (0, 0, 0) coordinate from any initial conditions. The dynamics equation in the new space is identical to that in Eq. (21). Substituting Eq. (24) into this dynamics equation results with the following optimal trajectory dynamics:

$$\dot{\bar{Z}}_1^*(t) = -\frac{N_{\text{ZEM}}}{t_{\text{go}}} \bar{Z}_1^*(t) - N_{\text{ZEAE}} v_M' \bar{Z}_2^*(t) \tag{34a}$$

$$\dot{\bar{Z}}_2^*(t) = \frac{N_{\text{ZEM}}}{v_M' t_{\text{go}}^2} \bar{Z}_1^*(t) + \frac{N_{\text{ZEAE}}}{t_{\text{go}}} \bar{Z}_2^*(t) \tag{34b}$$

The resulting equation set is a second-order linear time-variant ordinary differential equation (ODE) set. For the perfect intercept and perfect intercept angle case, for which $N_{\text{ZEM}} = 6$ and $N_{\text{ZEAE}} = 2$, the ODE set can be analytically solved yielding

$$\bar{Z}_1^*(t_{\text{go}}) = C_1 t_{\text{go}}^2 + C_2 t_{\text{go}}^3 \tag{35a}$$

$$\bar{Z}_2^*(t_{\text{go}}) = -\frac{2C_1}{v_M'} t_{\text{go}} - \frac{3C_2}{2v_M'} t_{\text{go}}^2 \tag{35b}$$

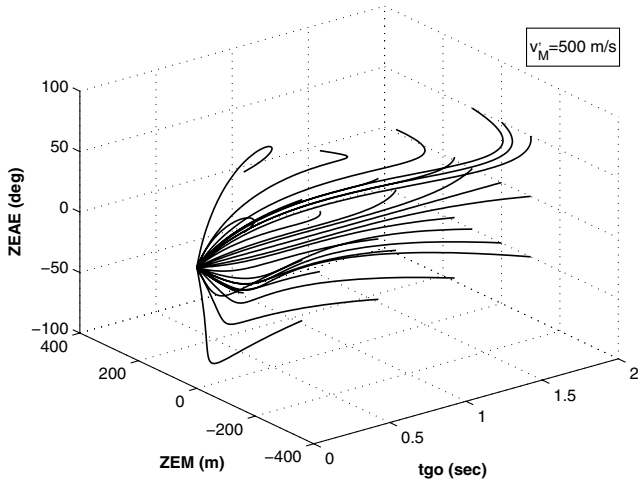

Fig. 3 OGL-CTIA perfect intercept ($a \to \infty$, $b \to \infty$) 3-D optimal trajectories.

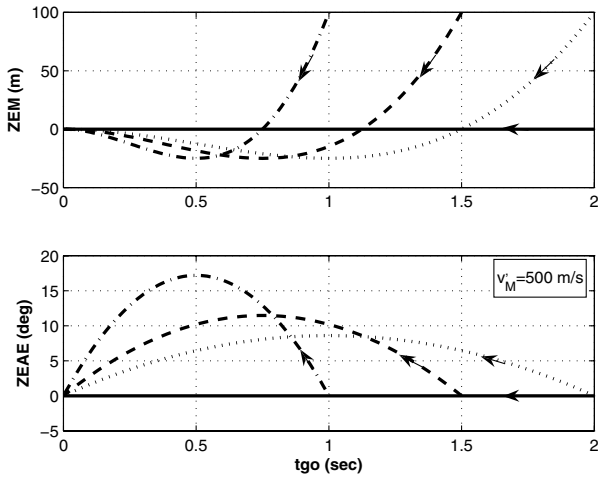

Fig. 4 OGL-CTIA perfect intercept ($a \to \infty$, $b \to \infty$) 2-D optimal trajectories.

where

$$C_1 = -\frac{3}{t_f^2}\bar{Z}_{10} - \frac{2v'_M}{t_f}\bar{Z}_{20}, \qquad C_2 = \frac{4}{t_f^3}\bar{Z}_{10} + \frac{2v'_M}{t_f^2}\bar{Z}_{20} \tag{36}$$

and $\bar{Z}_{10}$, $\bar{Z}_{20}$ are the initial conditions of $\bar{Z}_1$ and $\bar{Z}_2$, respectively. Figure 3 presents a 3-D plot of optimal trajectories from various initial conditions. It can be seen that all the optimal trajectories terminate in the (0, 0, 0) coordinate as expected and evident from the analytical solution. Note that we already proved in the previous section that the solution is optimal by showing that no conjugate point exists.

For presentation simplicity, Fig. 4 presents similar trajectories on a 2-D plot. The figure shows optimal trajectories from various initial ZEM values and with nulled ZEAE initial conditions. It can be seen that, to null the miss distance, the geometry is changed throughout the engagement and that the required angle is reached only at interception time.

IV. Linear Quadratic Differential Games Guidance Law

Unlike in the derivation of the optimal guidance law (Sec. III), in the differential game framework, we do not assume knowledge of the future target's maneuver strategy. We seek optimal strategies for both adversaries that satisfy a saddle point, that is, if one of the adversaries deviates from its optimal strategy then it cannot gain.

The quadratic cost function chosen for our zero-sum game is

$$J = \frac{a}{2}x_1^2(t_f) + \frac{b}{2}[x_4(t_f) - x_4^c]^2 + \frac{1}{2}\int_0^{t_f}(u^2 - \eta^2 w^2)\,\mathrm{d}t \tag{37}$$

where the weights a and b are nonnegative, and η represents the target's maneuvering capability relative to that of the missile. The projection of the target's acceleration command in the direction perpendicular to LOS_0 is $w = w_T\cos(\gamma_{T0} + \theta_0)$. The missile, using u as its control, wishes to minimize this cost function, whereas, the target, using w as its control, wishes to maximize it.

Remark: Similar to the integral cost on u^2 for the missile, an integral cost on w^2 is a common representation of the target's control effort [9]. For the same reasoning as that discussed in the preceding section for OGL, an equivalent representation, but with a running cost on u_M^2 and w_T^2, is also provided in the Appendix.

A. Order Reduction

Similar to the OGL case, we will use the terminal projection transformation to reduce the problem's order. To minimize the amount of indexing, we will use the same notation for the obtained new state vector $\mathbf{Z}$.

For this two-sided optimization problem, the transformation is

$$\mathbf{Z}(t) = \mathbf{D}\boldsymbol{\Phi}(t_f, t)\mathbf{x}(t) \tag{38}$$

The time derivative of the new variable $\mathbf{Z}(t)$ is

$$\dot{\mathbf{Z}} = \mathbf{D}\boldsymbol{\Phi}(t_f, t)\mathbf{B}u_M + \mathbf{D}\boldsymbol{\Phi}(t_f, t)\mathbf{C}w_T \tag{39}$$

which is independent of the states of the problem.

Using this new state vector $\mathbf{Z}(t)$, the cost function from Eq. (37) can also be expressed as

$$J = \frac{a}{2}Z_1^2(t_f) + \frac{b}{2}[Z_2(t_f) - x_4^c]^2 + \frac{1}{2}\int_0^{t_f}(u^2 - \eta^2 w^2)\,\mathrm{d}t \tag{40}$$

Note that, besides reducing the problem's order, the two coordinates of the new state vector $\mathbf{Z}(t)$ have a similar, but not identical, meaning as in the OGL case. $Z_1(t)$ is the ZEM, which is the miss distance if, from the current time onward, *both* the missile and the target will null their controls. $Z_2(t)$ is the ZEA, which is the intercept angle if, from the current time onward, *both* the missile and the target will not apply any controls.

B. Optimal Controllers

The Hamiltonian of the problem is

$$H = \frac{1}{2}u^2 - \frac{1}{2}\eta^2 w^2 + \lambda_1\dot{Z}_1 + \lambda_2\dot{Z}_2 \tag{41}$$

The adjoint equations and solutions are

$$\begin{cases} \dot{\lambda}_1 = -\frac{\partial H}{\partial Z_1} = 0; \quad \lambda_1(t_f) = aZ_1(t_f) \\ \dot{\lambda}_2 = -\frac{\partial H}{\partial Z_2} = 0; \quad \lambda_2(t_f) = b[Z_2(t_f) - x_4^c] \end{cases}$$
$$\Rightarrow \begin{cases} \lambda_1(t) = aZ_1(t_f) \\ \lambda_2(t) = b[Z_2(t_f) - x_4^c] \end{cases} \tag{42}$$

The optimal controllers for the missile and the target satisfy $u^* = \arg_u \min H$ and $w^* = \arg_w \max H$. As in the derivation of the OGL, we are seeking a closed-form solution for the control laws. Thus, we will assume dealing with ideal adversaries. This simplifies the time derivative of $\mathbf{Z}(t)$ to

$$\dot{\mathbf{Z}}(t) = \begin{bmatrix} -(t_f - t)\cos(\gamma_{M0} - \theta_0) \\ 1/V_M \end{bmatrix} u_M + \begin{bmatrix} (t_f - t)\cos(\gamma_{T0} + \theta_0) \\ 1/V_T \end{bmatrix} w_T \tag{43}$$

which can be rewritten as

$$\dot{\mathbf{Z}}(t) = \begin{bmatrix} -(t_f - t) \\ 1/v'_M \end{bmatrix} u + \begin{bmatrix} (t_f - t) \\ 1/v'_T \end{bmatrix} w \tag{44}$$

where $v'_T = V_T \cos(\gamma_{T0} + \theta_0)$ is the target's velocity component on LOS_0.

Remark: Note that, similar to the OGL case, when $\cos(\gamma_{M0} - \theta_0) \to 0$ or $\cos(\gamma_{T0} + \theta_0) \to 0$ the system is uncontrollable with respect to u_M or w_T, respectively. In such a case, the missile's or target's velocity vectors are perpendicular to the initial LOS and they do not have control authority in this direction. Using an integral cost on u_M and w_T, as in the alternative derivation given in the Appendix, can ensure that the navigation gains, as well as the controls u_M and w_T, are bounded for such a case.

For the considered ideal dynamics, the differential game guidance laws simplify to

$$\frac{\partial H}{\partial u} = 0 \Rightarrow u^*(t) = \lambda_1(t_f - t) - \lambda_2/v'_M \tag{45a}$$

$$\frac{\partial H}{\partial w} = 0 \Rightarrow w^*(t) = \frac{1}{\eta^2}[\lambda_1(t_f - t) + \lambda_2/v'_T] \tag{45b}$$

Using the same procedure as performed in the OGL derivation, we obtain

$$u^*(t) = \frac{N^u_{\mathrm{ZEM}}}{t^2_{\mathrm{go}}} Z_1(t) + N^u_{\mathrm{ZEAE}} \frac{v'_M}{t_{\mathrm{go}}}[Z_2(t) - x^c_4] \tag{46a}$$

$$w^*(t) = \frac{N^w_{\mathrm{ZEM}}}{t^2_{\mathrm{go}}} Z_1(t) + N^w_{\mathrm{ZEAE}} \frac{v'_M}{t_{\mathrm{go}}}[Z_2(t) - x^c_4] \tag{46b}$$

where

$$Z_1(t) = z + \dot{z} t_{\mathrm{go}} \tag{47a}$$

$$Z_2(t) = \gamma_T + \gamma_M \tag{47b}$$

and

$$N^u_{\mathrm{ZEM}} = \frac{3a\eta^2 t^3_{\mathrm{go}}}{\Delta_a} + \frac{bK_2(t_{\mathrm{go}})t^2_{\mathrm{go}}}{K_1(t_{\mathrm{go}})}\left(\frac{3a\eta^2 V_1 t^3_{\mathrm{go}}}{2\Delta_a} - \frac{1}{v'_M}\right) \tag{48a}$$

$$N^u_{\mathrm{ZEAE}} = \frac{bt_{\mathrm{go}}}{v'_M K_1(t_{\mathrm{go}})}\left(\frac{3a\eta^2 V_1 t^3_{\mathrm{go}}}{2\Delta_a} - \frac{1}{v'_M}\right) \tag{48b}$$

$$N^w_{\mathrm{ZEM}} = \frac{1}{\eta^2}\left[\frac{3a\eta^2 t^3_{\mathrm{go}}}{\Delta_a} + \frac{bK_2(t_{\mathrm{go}})t^2_{\mathrm{go}}}{K_1(t_{\mathrm{go}})}\left(\frac{3a\eta^2 V_1 t^3_{\mathrm{go}}}{2\Delta_a} + \frac{1}{v'_T}\right)\right] \tag{48c}$$

$$N^w_{\mathrm{ZEAE}} = \frac{bt_{\mathrm{go}}}{\eta^2 v'_M K_1(t_{\mathrm{go}})}\left(\frac{3a\eta^2 V_1 t^3_{\mathrm{go}}}{2\Delta_a} + \frac{1}{v'_T}\right) \tag{48d}$$

$$V_1 = \frac{v'_T\eta^2 + v'_M}{v'_M v'_T \eta^2}, \qquad V_2 = \frac{v'^2_M - v'^2_T\eta^2}{v'^2_M v'^2_T \eta^2}, \qquad \Delta_a = 3\eta^2 - (1-\eta^2)at^3_{\mathrm{go}} \tag{49}$$

$$K_1(t_{\mathrm{go}}) = 1 - bV_2 t_{\mathrm{go}} - \frac{3abV_1^2\eta^2 t^4_{\mathrm{go}}}{4\Delta_a}, \quad K_2(t_{\mathrm{go}}) = \frac{3aV_1\eta^2 t^2_{\mathrm{go}}}{2\Delta_a} \tag{50}$$

Similar to the OGL case, the closed-form solutions [presented in Eqs. (46)] of the optimal guidance laws for the two players are linear with respect to both the ZEM and the ZEAE. An asymptotic investigation of the navigation gains (N^u_{ZEM}, N^u_{ZEAE}, N^w_{ZEM}, N^w_{ZEAE}) shows that they are bounded when $v'_M \to 0$ or $v'_T \to 0$, and therefore u^* and w^* are also bounded in these cases.

The same implementation requirements as for OGL apply to the LQDG derived in this section, with the exception that the target's acceleration is not required in this case. However, if non-zero-lag dynamics were assumed for the target, then its acceleration would have been needed for the implementation. The same is true for the missile.

C. Navigation Gains

Let us now examine the values of the navigation gains derived in Eqs. (48). By choosing $b \to 0$, we no longer impose an intercept angle, resulting in

$$N^u_{\mathrm{ZEM}}(b \to 0) = \frac{3a\eta^2 t^3_{\mathrm{go}}}{3\eta^2 - (1-\eta^2)at^3_{\mathrm{go}}}, \qquad N^u_{\mathrm{ZEAE}}(b \to 0) = 0 \tag{51a}$$

$$N^w_{\mathrm{ZEM}}(b \to 0) = \frac{3at^3_{\mathrm{go}}}{3\eta^2 - (1-\eta^2)at^3_{\mathrm{go}}}, \qquad N^w_{\mathrm{ZEAE}}(b \to 0) = 0 \tag{51b}$$

and the degeneration of the guidance laws in Eqs. (46) to the LQDG presented in [9].

If we also choose $a \to \infty$, which dictates zero miss, the navigation gains further degenerate to

$$N^u_{\mathrm{ZEM}}(b \to 0, a \to \infty) = \frac{3\eta^2}{(\eta^2 - 1)}, \qquad N^u_{\mathrm{ZEAE}}(b \to 0, a \to \infty) = 0 \tag{52a}$$

$$N^w_{\mathrm{ZEM}}(b \to 0, a \to \infty) = \frac{3}{(\eta^2 - 1)}, \qquad N^w_{\mathrm{ZEAE}}(b \to 0, a \to \infty) = 0 \tag{52b}$$

also presented in [9]. And, by considering a nonmaneuvering target scenario ($\eta \to \infty$), we get the well-known optimal PN guidance law with $N^u_{\mathrm{ZEM}} = 3$. For a perfect intercept with some account for terminal intercept angle, we would require $a \to \infty$ and a finite b, resulting in the following navigation gains

$$N^u_{\mathrm{ZEM}}(a \to \infty) = \frac{3\eta^2}{(\eta^2 - 1)} + \frac{6b\eta^2 V_1 t_{\mathrm{go}}}{\Delta_b}\left(\frac{3\eta^2 V_1}{2(1-\eta^2)} + \frac{1}{v'_M}\right) \tag{53a}$$

$$N^u_{\mathrm{ZEAE}}(a \to \infty) = \frac{4b(\eta^2 - 1)t_{\mathrm{go}}}{v'_M \Delta_b}\left(\frac{3\eta^2 V_1}{2(1-\eta^2)} + \frac{1}{v'_M}\right) \tag{53b}$$

$$N^w_{\mathrm{ZEM}}(a \to \infty) = \frac{3}{(\eta^2 - 1)} + \frac{6bV_1 t_{\mathrm{go}}}{\Delta_b}\left(\frac{3\eta^2 V_1}{2(1-\eta^2)} - \frac{1}{v'_T}\right) \tag{53c}$$

$$N^w_{\mathrm{ZEAE}}(a \to \infty) = \frac{4b(\eta^2 - 1)t_{\mathrm{go}}}{v'_M \eta^2 \Delta_b}\left(\frac{3\eta^2 V_1}{2(1-\eta^2)} - \frac{1}{v'_T}\right) \tag{53d}$$

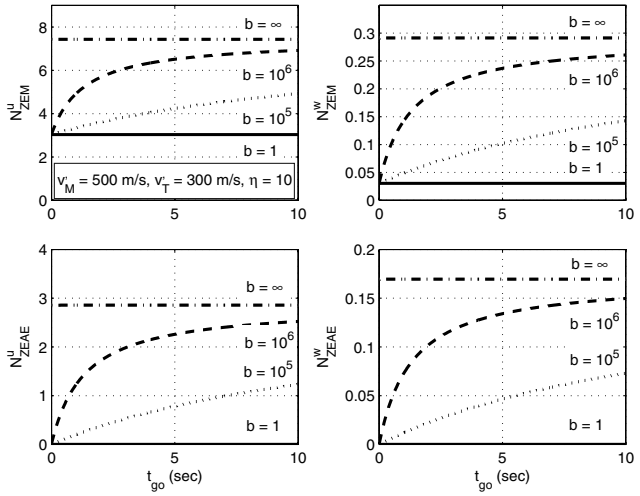

Fig. 5 LQDG-CTIA navigation gains for perfect intercept ($a \to \infty$) and $\eta = 10$.

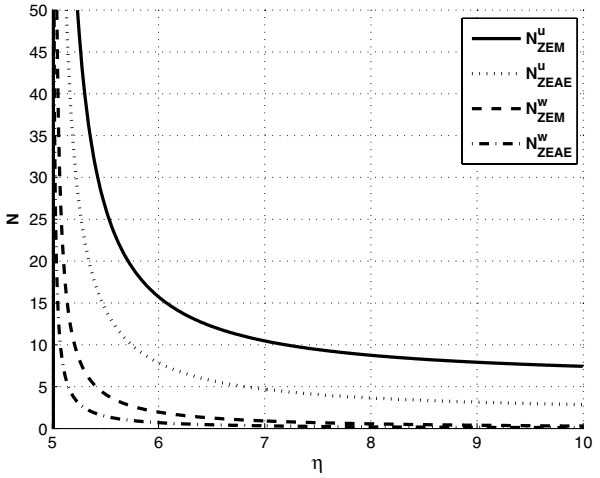

Fig. 6 LQDG-CTIA navigation gains for perfect intercept and intercept angle.

where

$$\Delta_b = 4(1-\eta^2) + bt_{\text{go}}[3\eta^2 V_1^2 - 4(1-\eta^2)V_2] \tag{54}$$

Figure 5 presents the time history of the navigation gains for a perfect intercept, $\eta = 10$, and a few representative values of b. Note that the navigation gains are constant with respect to t_{go} for $b \to 0$ and $b \to \infty$ and increase with t_{go} for values of b in between, similar to what we have seen in the OGL case.

The weight η is a design parameter associated with the expected maneuvering capability perpendicular to LOS_0 of the target compared with the interceptor. Thus, for smaller values of η (a more maneuverable target), larger gains are obtained. If the target is not expected to maneuver, a large value of η should be chosen and vise versa. Imposing a perfect intercept and intercept angle (or large values of a and/or b to improve performance, for that matter) might result in a conjugate point. In such a case, to obtain a solution in the entire game space, performance must be compromised by using smaller values of a and b.

A conjugate point does not exist if and only if the gains are finite [9] for all $0 < t_{\text{go}} \le t_f$. For example, in Eq. (52), the gains diverge for $\eta = 1$, therefore a conjugate point exists for $|\eta| \le 1$ and the solution is no longer optimal. The critical value of η is denoted η_{cr}, and, to avoid a conjugate point, we must select $|\eta| > \eta_{\text{cr}}$.

For a perfect intercept and perfect intercept angle we would require both a and b to approach infinity ($a, b \to \infty$), resulting in the degeneration of the navigation gains of Eqs. (48) to

$$N^u_{\text{ZEM}}(a, b \to \infty) = \frac{6\eta^2}{\Delta_\infty}\left(2V_2 + \frac{V_1}{v'_M}\right) \tag{55a}$$

$$N^u_{\text{ZEAE}}(a, b \to \infty) = -\frac{1}{v'^2_M \Delta_\infty}[6\eta^2 V_1 v'_M + 4(1-\eta^2)] \tag{55b}$$

$$N^w_{\text{ZEM}}(a, b \to \infty) = \frac{6}{\Delta_\infty}\left(2V_2 - \frac{V_1}{v'_T}\right) \tag{55c}$$

$$N^w_{\text{ZEAE}}(a, b \to \infty) = -\frac{1}{v'_M v'_T \eta^2 \Delta_\infty}[6\eta^2 V_1 v'_T - 4(1-\eta^2)] \tag{55d}$$

where

$$\Delta_\infty = 3V_1^2\eta^2 - 4V_2(1-\eta^2) \tag{56}$$

Note that the navigation gains for the $a, b \to \infty$ case are not a function of the time to go, similar to what we have seen for the OGL case.

Figure 6 presents the navigation gains for perfect intercept and perfect intercept angle ($a,\ b \to \infty$) for $v'_M = 500$ m/s, and $v'_T = 300$ m/s. Clearly, as $\eta \to 5$, the gains diverge. The navigation gains for this case are unbounded when $\Delta_\infty \to 0$, therefore, if there exists a η_{cr} for which $\Delta_\infty(\eta_{\text{cr}}) \to 0$, then a conjugate point exists for $|\eta| \le \eta_{\text{cr}}$ and the solution may not be optimal. For this sample case, $\eta_{\text{cr}} = 5$ and, consequently, a conjugate point exists for $|\eta| \le 5$. We will derive the conditions for the existence of an optimal solution for the perfect intercept and perfect intercept angle case in the next subsection.

By assuming a nonmaneuvering target scenario ($\eta \to \infty$), the navigation gains further degenerate to

$$N^u_{\text{ZEM}}(a, b, \eta \to \infty) = 6, \qquad N^u_{\text{ZEAE}}(a, b, \eta \to \infty) = 2 \tag{57a}$$

$$N^w_{\text{ZEM}}(a, b, \eta \to \infty) = 0, \qquad N^w_{\text{ZEAE}}(a, b, \eta \to \infty) = 0 \tag{57b}$$

Note that the missile's navigation gains retain the values obtained in the OGL case [Eq. (32)] and, obviously, in this scenario, the target's gains are nulled.

D. Perfect Intercept and Perfect Intercept Angle

Using the LQDG guidance law, we can guarantee perfect intercept and perfect intercept angle, provided a solution exists. As we have seen in the previous section, a conjugate point may exist in some scenarios. In such scenarios, an optimal solution to the game might not exist for some $t_{\text{go}} \ge 0$. In this section, we will present the optimal trajectories obtained for the perfect intercept and intercept angle case, and study the conditions for the existence of a solution to the differential game.

Let us perform a similar transformation to the one we have performed in the OGL case

$$\bar{\mathbf{Z}}(t) = \begin{bmatrix} Z_1(t) \\ Z_2(t) - x_4^c \end{bmatrix} \tag{58}$$

Like in the OGL case, the new state vector $\bar{\mathbf{Z}}(t)$ uses the ZEAE as the second state instead of the ZEA. The dynamic equation in the new space is the same as in Eq. (44) for the original state vector $\mathbf{Z}(t)$. Substituting Eqs. (46) into this equation yields the following optimal trajectory dynamics:

$$\dot{\bar{Z}}_1^*(t) = (N^w_{\text{ZEM}} - N^u_{\text{ZEM}})\frac{\bar{Z}_1^*(t)}{t_{\text{go}}} + (N^w_{\text{ZEAE}} - N^u_{\text{ZEAE}})v'_M \bar{Z}_2^*(t) \tag{59a}$$

$$\dot{\bar{Z}}_2^*(t) = \left(\frac{N^u_{\mathrm{ZEM}}}{v'_M} + \frac{N^w_{\mathrm{ZEM}}}{v'_T}\right)\frac{\bar{Z}_1^*(t)}{t_{\mathrm{go}}^2} + \left(N^u_{\mathrm{ZEAE}} + \frac{v'_M}{v'_T}N^w_{\mathrm{ZEAE}}\right)\frac{\bar{Z}_2^*(t)}{t_{\mathrm{go}}} \tag{59b}$$

The resulting equation set is a second-order linear time-variant ODE set. For the perfect intercept and perfect intercept angle case, N^u_{ZEM}, N^u_{ZEAE}, N^w_{ZEM}, and N^w_{ZEAE} have been shown to be constant with respect to time [see Eq. (55)], and the ODE set can be analytically solved yielding

$$\begin{aligned}\bar{Z}_1^*(t) &= C_3 t_{\mathrm{go}}^{\alpha} + C_4 t_{\mathrm{go}}^{\beta},\\ \bar{Z}_2^*(t) &= \frac{(\alpha - a_{11})}{a_{12}} C_3 t_{\mathrm{go}}^{\alpha-1} + \frac{(\beta - a_{11})}{a_{12}} C_4 t_{\mathrm{go}}^{\beta-1}\end{aligned} \tag{60}$$

where

$$a_{11} = (N^u_{\mathrm{ZEM}} - N^w_{\mathrm{ZEM}}), \qquad a_{12} = (N^u_{\mathrm{ZEAE}} - N^w_{\mathrm{ZEAE}})v'_M \tag{61a}$$

$$a_{21} = -\left(\frac{N^u_{\mathrm{ZEM}}}{v'_M} + \frac{N^w_{\mathrm{ZEM}}}{v'_T}\right), \qquad a_{22} = -\left(N^u_{\mathrm{ZEAE}} + \frac{v'_M}{v'_T}N^w_{\mathrm{ZEAE}}\right) \tag{61b}$$

and

$$\delta = \sqrt{(a_{11} - a_{22})^2 - 2(a_{11} - a_{22}) + 4a_{12}a_{21} + 1} \tag{62a}$$

$$\alpha = \frac{1}{2}(a_{11} + a_{22} + 1 + \delta) \tag{62b}$$

$$\beta = \frac{1}{2}(a_{11} + a_{22} + 1 - \delta) \tag{62c}$$

$$C_3 = \frac{1}{t_f^{\alpha}}\left[\left(1 - \frac{\alpha - a_{11}}{\delta}\right)\bar{Z}_{10} + \left(\frac{a_{12}t_f}{\delta}\right)\bar{Z}_{20}\right] \tag{62d}$$

$$C_4 = \frac{1}{t_f^{\beta}}\left[\left(\frac{\alpha - a_{11}}{\delta}\right)\bar{Z}_{10} - \left(\frac{a_{12}t_f}{\delta}\right)\bar{Z}_{20}\right] \tag{62e}$$

for which $\bar{Z}_{10}$ and $\bar{Z}_{20}$ are the initial conditions of $\bar{Z}_1$ and $\bar{Z}_2$, respectively.

Figure 7 presents a 3-D plot (t_{go}, ZEM, ZEAE) of optimal trajectories from various initial conditions. It can be seen that all the optimal trajectories terminate at the (0, 0, 0) coordinate as expected. Figure 8 presents similar trajectories on a 2-D plot. The optimal trajectories start with various nonzero initial ZEM values and with nulled ZEAE initial conditions. Compared to Fig. 4 obtained for OGL, it can be seen that throughout the engagement ZEM and ZEAE reach larger values. This can be attributed to the larger gains used in the LQDG guidance law.

Thus far, we have shown trajectories emerging from a saddle-point solution of the game. As we have seen in the previous section, a conjugate point may exist, in which case, the solution might not be optimal any more. The nonexistence of a conjugate point has been shown to be a sufficient condition for the existence of a saddle-point solution to the game [9]. A conjugate point exists if and only if $\mathbf{P}(t)$ of the Riccati equation associated with the original problem is not finite [8]:

$$\dot{\mathbf{P}} = \mathbf{P}\mathbf{A}\mathbf{A}^T\mathbf{P} + \mathbf{P}(\eta^{-2}\mathbf{C}\mathbf{C}^T - \mathbf{B}\mathbf{B}^T)\mathbf{P}; \qquad \mathbf{P}(t_f) = \mathbf{Q}_f \tag{63}$$

The same is true of course for the reduced-order problem. In turn, $\mathbf{P}(t)$ is finite if and only if the solution navigation gains are bounded

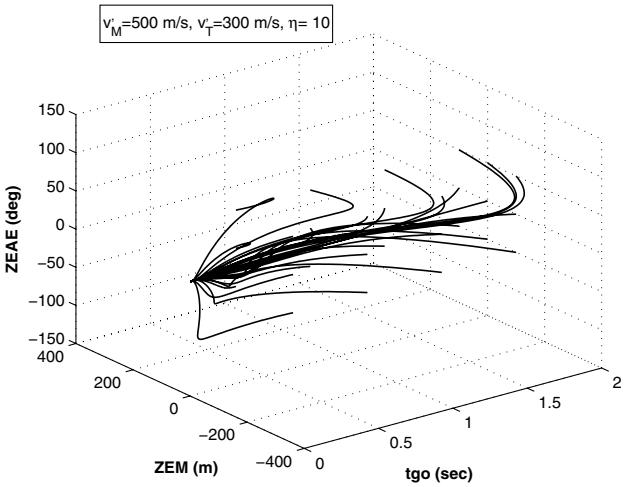

Fig. 7 LQDG-CTIA perfect intercept ($a \to \infty$, $b \to \infty$) 3-D optimal trajectories, without a conjugate point.

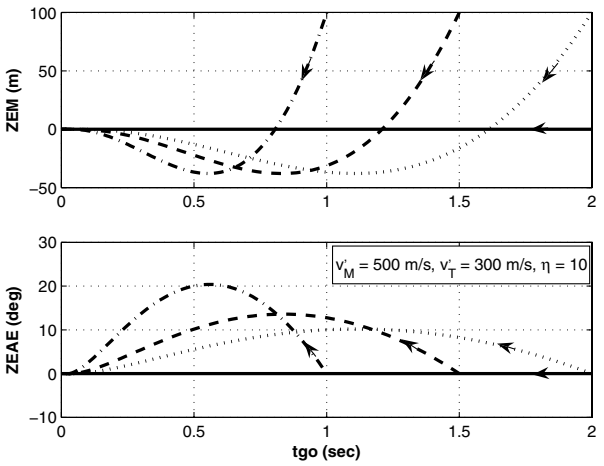

Fig. 8 LQDG-CTIA perfect intercept ($a \to \infty$, $b \to \infty$) 2-D optimal trajectories, without a conjugate point.

[9]. Therefore, a saddle point exists if the navigation gains are bounded.

Let us now consider the conditions for the existence of a conjugate point in the perfect intercept and intercept angle scenario. As we have seen in the previous section, the navigation gains are unbounded when $\Delta_\infty \to 0$, where Δ_∞ is defined in Eq. (56). By substituting the definitions of V_1 and V_2 from Eqs. (49) into Eq. (56), we obtain

$$\Delta_\infty = \frac{1}{v'^2_M v'^2_T \eta^2}[3(v'_T\eta^2 + v'_M)^2 - 4(v'^2_M - v'^2_T\eta^2)(1 - \eta^2)] \tag{64}$$

and, by equating the result to zero and reordering, we can find the values of η that satisfy $\Delta_\infty(\eta) = 0$:

$$-v'^2_T\eta^4 + [4(v'^2_M + v'^2_T) + 6(v'_T v'_M)]\eta^2 - v'^2_M = 0 \tag{65}$$

This quadratic equation in η^2 obviously has a maximum. By substituting $\eta^2 = 0$ and $\eta^2 = 1$ in Eq. (65), we get $-v'^2_M$ and $3(v'^2_M + v'^2_T)$, respectively. We can therefore conclude that the equation has two roots: the first $\eta^2 < 1$ and the second $\eta^2 > 1$. We define η_∞ as the larger root between the two, and a conjugate point does not exist in this case for $1 < \eta_\infty < |\eta|$. Let us now prove that a conjugate point exists for $|\eta| \le \eta_\infty$.

First, consider the general case for any value of the weights a and b. It is apparent from Eq. (48) that N^u_{ZEM} and N^w_{ZEM} are unbounded when $\Delta_a \to 0$, where Δ_a is defined in Eq. (49). By equating Δ_a to zero, we can derive the conditions for which the gains are unbounded and therefore a conjugate point exists:

$$\Delta_a = 3\eta^2 - (1-\eta^2)at_{\text{go}}^3 = 0 \tag{66}$$

The critical t_{go}, denoted $[t_{\text{go}}^{\text{cr}}]_a$, from Eq. (66) is

$$[t_{\text{go}}^{\text{cr}}]_a = \arg_{t_{\text{go}}}[\Delta_a(t_{\text{go}}) = 0] = \sqrt[3]{\frac{3\eta^2}{(1-\eta^2)a}} \tag{67}$$

Therefore, for every $|\eta| < 1$, and for every positive value of a, there exists a nonnegative $[t_{\text{go}}^{\text{cr}}]_a$ for which $\Delta_a \to 0$, and, consequently, the navigation gains of Eqs. (48) are unbounded at that t_{go}. The conjugate point only appears in scenarios lasting $t_f \geq [t_{\text{go}}^{\text{cr}}]_a$, and it emerges for *all* positive values of a and nonnegative values b. For the perfect intercept case $[t_{\text{go}}^{\text{cr}}]_a(a \to \infty) \to 0$.

Let us now consider the perfect intercept case without requiring a perfect intercept angle. In that case, the navigation gains are unbounded when $\Delta_b \to 0$, where Δ_b is defined in Eq. (54). By equating Δ_b to zero and substituting Eq. (56), we can derive the conditions for which the gains are unbounded:

$$\Delta_b = 4(1-\eta^2) + bt_{\text{go}}\Delta_\infty = 0 \tag{68}$$

The critical t_{go}, denoted $[t_{\text{go}}^{\text{cr}}]_b$, from Eq. (68) is

$$[t_{\text{go}}^{\text{cr}}]_b = \arg_{t_{\text{go}}}[\Delta_b(t_{\text{go}}) = 0] = -\frac{4(1-\eta^2)}{b\Delta_\infty} \tag{69}$$

It is apparent from Eqs. (64) and (69) that, for every $1 \leq |\eta| \leq \eta_\infty$, and for every positive b, there exists a nonnegative $[t_{\text{go}}^{\text{cr}}]_b$ for which $\Delta_b \to 0$, and therefore the navigation gains of Eq. (53) are unbounded at that t_{go}. This means that, for a perfect intercept without a perfect intercept angle constraint ($a \to \infty$, $b < \infty$) with $1 \leq |\eta| \leq \eta_\infty$, a conjugate point does not exist for scenarios lasting $0 < t_f < [t_{\text{go}}^{\text{cr}}]_b$. On the other hand, a conjugate point exists for scenarios in which $t_f \geq [t_{\text{go}}^{\text{cr}}]_b$. For the perfect intercept and intercept angle case, $[t_{\text{go}}^{\text{cr}}]_b(a \to \infty, b \to \infty) \to 0$. We can hence conclude from Eqs. (67) and (69) that, for every $|\eta| \leq \eta_\infty$, a conjugate point exists and that, for the perfect intercept and intercept case, $t_{\text{go}}^{\text{cr}} \to 0$, and therefore the claim is proven.

Figure 9 presents the values of η_∞ as a function of v'_M and v'_T. Note that the maneuver advantage required for the missile over the target is smaller when v'_M, the missile's velocity component on LOS_0, is smaller. The intercept angle is controlled by changing the path angle γ_M according to $\dot{\gamma}_M = a_{\text{MN}}/(v'_M)$. Therefore, it is clear that, for a slower missile, the needed acceleration to control the path angle is smaller. This analysis does not consider the ability of the missile to generate the required acceleration, which, in aerodynamically controlled missiles, is obviously a function of the missile's lift, which in turn is a function of the missile's velocity.

Figure 10 presents the maximal scenario duration for a perfect intercept game for $v'_M = 500$ m/s, and $v'_T = 300$ m/s. The figure presents $t_{\text{go}}^{\text{cr}}$ as a function of the selected values of the design parameters η and b. As expected, we can obtain a saddle-point solution for the game for practical engagement scenarios by compromising intercept angle performance. We can also see that, for small values of b, we converge to the well-known LQDG solution, for which $\eta_{\text{cr}} = 1$. Another interesting observation that arises from Fig. 10 is that adding a requirement on the intercept angle, by increasing the value of b, dramatically increases the maneuvering advantage needed by the missile over the target. This is not surprising, because the interceptor needs to reshape its trajectory to generate the required angle for every change in the target's path angle. This result limits the usefulness of the proposed guidance law to missiles with high maneuvering capability with respect to the intercepted targets. This observation holds for the OGL case as well, as will be seen in the next section.

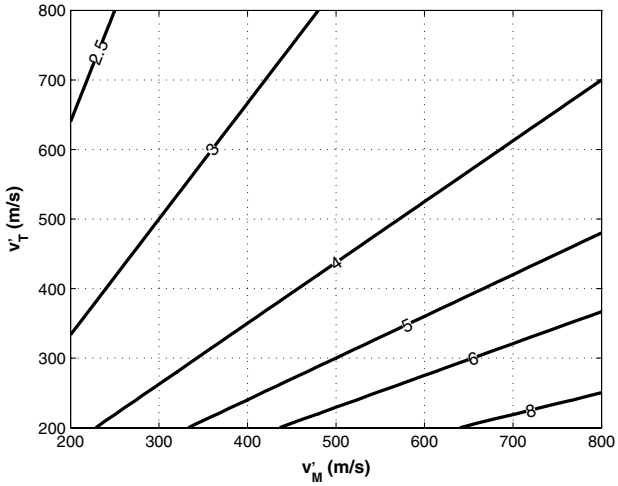

Fig. 9 LQDG-CTIA conditions on η for perfect intercept and intercept angle ($a, b \to \infty$).

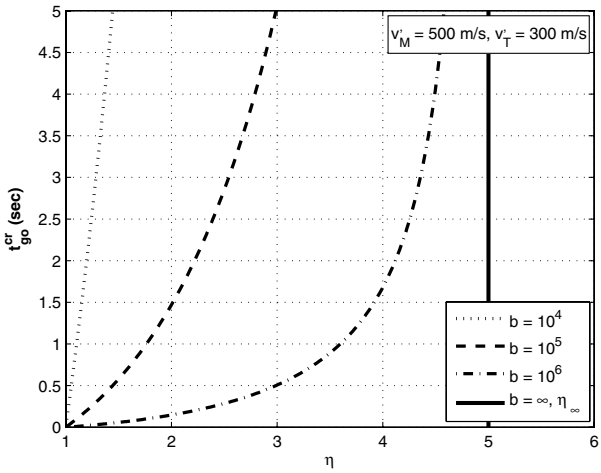

Fig. 10 LQDG-CTIA maximal scenario duration for perfect intercept ($a \to \infty$).

V. Performance Analysis

Performance of the two guidance laws developed in Secs. III and IV is investigated in this section via numerical simulations, using the nonlinear kinematics and missile and target dynamics presented in Sec. II.A. We will first outline the nonlinear test scenarios, then demonstrate and investigate the performance of each guidance law in a nonlinear simulation, and finally will compare the OGL-CTIA and LQDG-CTIA using a Monte Carlo study.

A. Scenarios

Two interception scenarios are used for the performance analysis. The first scenario, in which the target performs a constant maneuver, will be used to demonstrate and evaluate each guidance law separately. This scenario was chosen due to its simplicity and ease of presentation. The second scenario, in which the target performs a random evasive maneuver, will be used in our Monte Carlo study to compare and evaluate the LQDG-CTIA and OGL-CTIA laws in a more realistic setting. The latter scenario is based on the test scenario presented in [10].

The engagements are initiated in head-on setting. The vehicles are not necessarily initially flying along the required collision triangle. Thus, we continuously update γ_{M0}, γ_{T0}, and θ_0 used for the guidance law implementation. The initial range is 2000 m. The target speed is $V_T = 300$ m/s and its maneuver capability is $a_T = 5g$. We will use a missile and target first-order time constants of $\tau_M = 0.1$ s and $\tau_T = 0.1$ s, respectively. In the first scenario, $V_M \in \{300, 500, 700\}$ m/s and the target is performing a constant maximum maneuver. In the second scenario, the missile's speed is 500 m/s and the target performs a square wave evasive maneuver (using its maximum acceleration capability) with a period of ΔT and a phase of $\Delta\phi$ relative to the beginning of the simulation. Because of the soft

limit nature of the control law derivation, we will not impose a saturation value in the simulation, but we will comment on the missile's maximal acceleration values during the analysis.

B. Optimal Guidance Law Performance

We first present the ability of the proposed OGL to intercept the target in the required angle. Figure 11 presents the trajectories obtained while using the OGL-CTIA guidance law (note the different scaling in the X and Z axis). By choosing $x_4^c = \gamma_T + \gamma_M = 0$, the commanded intercept angle is head-on . When $b \to 0$, the trajectories coincide with those obtained using the classic OGL. When the weight b is increased, the missile's trajectory is shaped to intercept the target in the required intercept angle. Consequently, as b is increased, the final intercept angle error is decreased from about 35 deg, when $b = 1$ (which is virtually the same as the classic OGL obtained for $b = 0$), to less than 1 deg for $b = 10^8$. This is expected from the formulation of the guidance law, but this does not come without a price. The missile's maximal acceleration is increased from $a_M^{\max} \approx 7.5g$ to $a_M^{\max} \approx 45g$, with the maximal acceleration being at the end of the engagement instead of the beginning of the engagement, which is usually unwanted. The large acceleration ratio between the missile and the target is mainly due to the large angle correction required due to the target maneuver (no initial angle error was present in this case). It is therefore expected that high values of η will be needed in the LQDG formulation to avoid a conjugate point. One important conclusion that can be deducted is that, for the implementation of this guidance law, a substantial acceleration advantage is needed.

The weights a and b are design parameters reflecting a tradeoff between the allowable miss distance, intercept angle error, and lateral acceleration. We have chosen $a = 10^5$ and $b = 10^8$ for most simulation runs. These values were selected to give equal weight to approximately 1 m in miss distance, 2 deg in intercept angle, and $25g$ in sustained acceleration for a scenario duration of 2 s.

Figure 12 presents trajectories for different requirements on the intercept angle. The scenario is the same as before, with $a = 10^5$ and $b = 10^8$. The miss distances and intercept angle errors were very small in these runs. The worst miss distance in the tested range was approximately 0.17 m, and the worst intercept angle error was approximately 2 deg. Note that the nominal interception angle using a basic OGL is approximately 35 deg, as can be seen in Fig. 11. Therefore, it is expected that the miss distance and intercept angle error close to that nominal angle would be the smallest, as is apparent in Fig. 13. Similar results have been obtained for different initial heading errors. Note that, although we demonstrated the guidance law's capability to correct initial intercept angle errors, such angle errors should be addressed in the midcourse phase of the engagement and not left to the endgame in which higher accelerations will be required, due to the shorter time remaining.

Figure 14 presents the sensitivity of the guidance law to the missile's speed V_M. In these runs, the peak accelerations increased as the missile's speed increased, being approximately 40, 45, and $58g$ for speeds of 300, 500, and 700 m/s, respectively. The reasoning for this was expansively explained in Sec. IV, and the same logic holds for this guidance law as well. During the theoretical derivation of the LQDG-CTIA guidance law in Sec. IV, we have noted that a conjugate point exists at larger values of η when the missile's speed component on the initial LOS v'_M is larger. This suggested that larger missile accelerations are required when v'_M is increased. We have not seen an obvious parallel to this in the theoretical derivation of the OGL-CTIA.

C. Differential Game Guidance Law Performance

Unlike the OGL case, in the LQDG formulation, we have an additional design parameter η, which is related to the target's maneuvering capability compared with that of the missile. As we have seen in the theoretical analysis of this guidance law, for $v'_M = 500$ m/s and $v'_T = 300$ m/s, we obtain $\eta_\infty = 5$, and a saddle point exists for $|\eta| > \eta_\infty$. Figure 15 presents the same engagement scenario as in the previous subsection with different values of

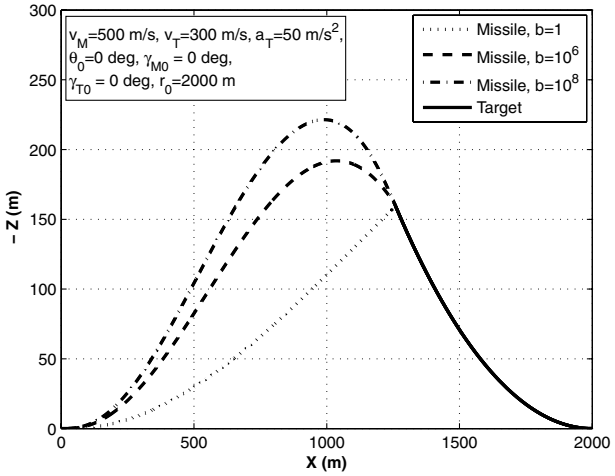

Fig. 11 OGL-CTIA trajectories for various values of b; $x_4^c = 0$, $a = 10^5$.

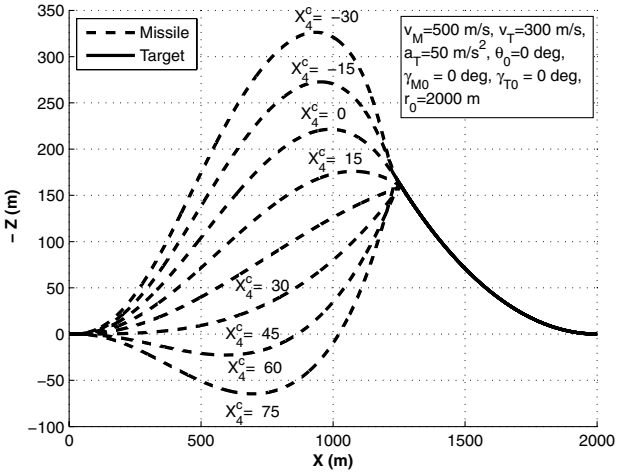

Fig. 12 OGL-CTIA trajectories for various intercept angle commands; $a = 10^5$, $b = 10^8$.

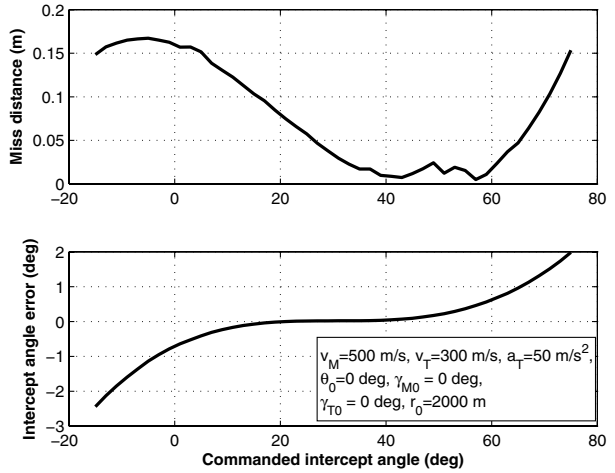

Fig. 13 OGL-CTIA intercept performance for various intercept angle commands; $a = 10^5$, $b = 10^8$.

$|\eta| > 5$. For the different values of η, interception is obtained with the required terminal angle. The difference is in the required maximal missile acceleration and with the changing engagement geometry. As η increases, the maximal missile acceleration increases as well,

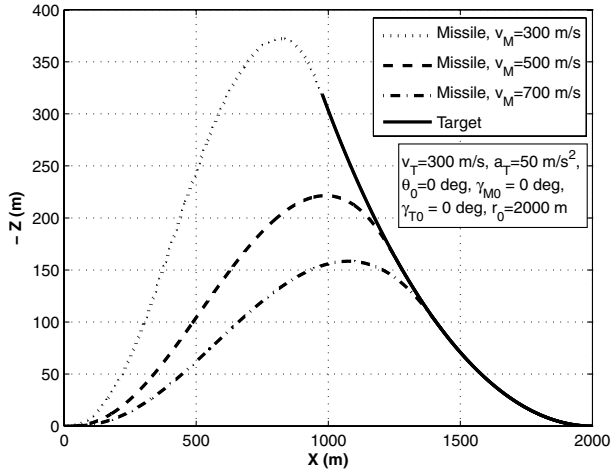

Fig. 14 OGL-CTIA trajectories for various missile speeds; $x_4^c = 0$, $a = 10^5$, $b = 10^8$.

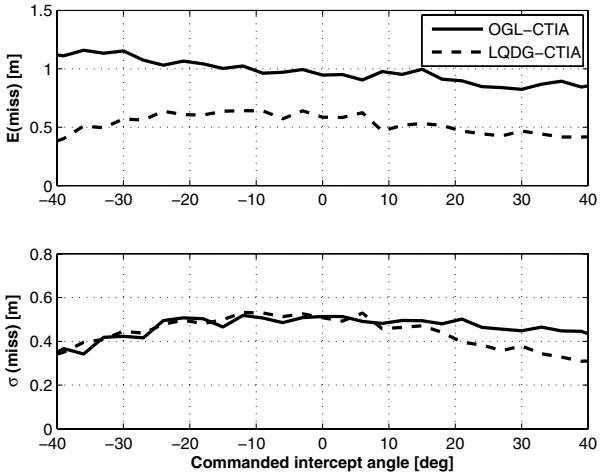

Fig. 16 Miss distance for various intercept angles; $a = 10^5$, $b = 10^8$, $\eta = 7$, $\Delta T = 2$ s, $\Delta\phi = [0, 1]$.

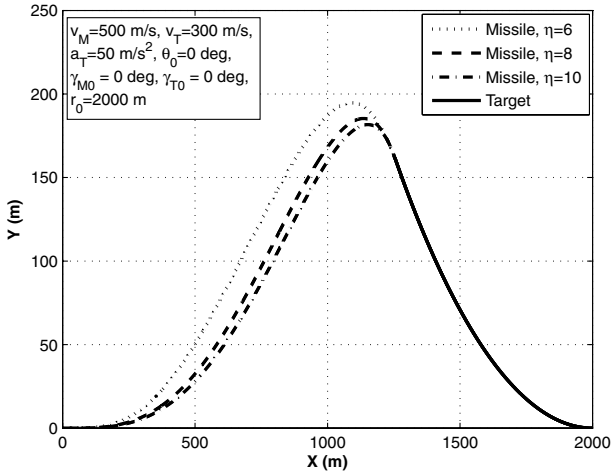

Fig. 15 LQDG-CTIA trajectories for various values of η; $x_4^c = 0$, $a = 10^5$, $b = 10^8$.

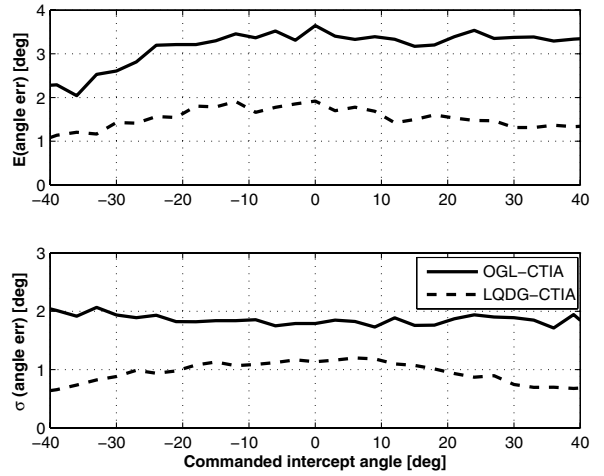

Fig. 17 Intercept angle error for various intercept angles; $a = 10^5$, $b = 10^8$, $\eta = 7$, $\Delta T = 2$ s, $\Delta\phi = [0, 1]$.

from approximately $65g$ for $\eta = 6$ to $120g$ for $\eta = 10$. This is because, when η is higher, lower gains are employed at the beginning of the engagement, resulting in higher corrections required at the end of the engagement, where the maximal acceleration usually occurs. It is obvious that this parameter needs to be maintained as small as possible to reduce the possibility of control saturation, but it is dependent on the expected missile-to-target maneuver capability ratio.

Qualitatively similar results have been obtained with regard to Figs. 11–14, presented for OGL. These are not shown here for the sake of conciseness. Note that the maximal accelerations obtained using this guidance law are larger than in the OGL case. This is also expected, due to the scenario we are analyzing. In our engagement scenario, the target performs a constant turn, and the OGL is formulated to be optimal for this exact maneuver, whereas the LQDG is not.

D. Optimal Guidance Law/Differential Game Guidance Law Performance Comparison

Thus far, we have evaluated each guidance law in a scenario where the target is performing a constant maneuver. In actual engagements, the target might perform unpredictable evasive maneuvers. Also, a constant maneuver scenario is unsuitable to compare the performance of OGL and LQDG, as OGL was derived specifically for this maneuver and LQDG was not. Therefore, we will evaluate and compare the two guidance laws in a different scenario, presented in Sec. V.A, in which the target performs a square wave evasive maneuver, with a period of ΔT and a phase of $\Delta\phi$.

To evaluate and compare the two guidance laws, a Monte Carlo study consisting of 200 simulation runs for each test point was performed. In these simulations, for each sample run, a random value was chosen for $\Delta\phi$ from a uniform distribution, in the range $\Delta\phi = [0, 1]$. The period was chosen to be $\Delta T = 2$ s. To properly compare the two guidance laws, the statistics (mean and standard deviation) of all the components of the cost function were evaluated.

Figures 16–18 present the statistics of the miss distance, intercept angle error, and the control effort, respectively, as a function of the commanded intercept angle. It is clear that the two guidance laws, OGL and LQDG, yield good performance with an expected miss of approximately 1 and 0.5 m and an expected angle error of approximately 3 and 1.5 deg, respectively. The LQDG law outperforms the OGL in this scenario in all the evaluated cost measures. This is expected because the target is not performing the constant maneuver assumed in the OGL derivation. Performing the same analysis in the constant target maneuver scenario yields opposite results. It is also clear that the miss and intercept angle error are only moderately effected by the commanded intercept angle, whereas the control effort is larger for larger intercept angle requirements. The increase in control effort for large intercept angles is expected, due to the larger curvature and longer trajectories required in these cases.

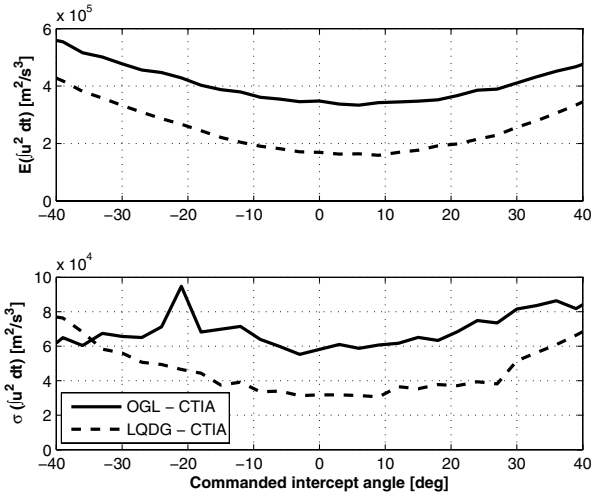

Fig. 18 Control effort for various intercept angles; $a = 10^5$, $b = 10^8$, $\eta = 7$, $\Delta T = 2$ s, $\Delta\phi = [0, 1]$.

VI. Conclusions

In this paper, two guidance laws which enable imposing a predetermined terminal intercept angle were developed using linear quadratic optimal control and differential games methodologies. The navigation gains of two closed-form solutions were studied, and their behavior was analyzed for the perfect intercept and perfect intercept angle case. Optimal trajectory equations for this case were derived, analytically solved, and plotted, and analytical conditions for the existence of a saddle point solution in the differential game were derived. The analysis and simulations indicate that the two guidance laws exhibit very small miss distances and intercept angle errors, provided a large missile-to-target maneuver capability exists. The linear quadratic optimal control guidance law is best suited when the target maneuver is known, and the linear quadratic differential game guidance law is more appropriate when the target maneuver is unpredictable, making the optimal choice scenario dependent. Even when the scenario was initiated with large deviations from the collision triangle and the target performed a hard maneuver, causing large deviations from an initial collision triangle, the guidance laws exhibited excellent performance by providing near-zero miss distance and intercept angle error. The capability demonstrated by these guidance laws to impose an intercept angle can greatly improve the interceptor's warhead lethality, resulting in possible warhead size reduction. It may also decrease the target's ability to effectively employ countermeasures.

Appendix: Equivalent Derivation

The guidance law derived in Sec. III included an integral cost on u^2, whereas the guidance law derived in Sec. IV included integral costs on both u^2 and w^2. These are common representations of the missile's and target's control efforts [9,12]. When $|\gamma_{M0} - \theta_0|$ and/or $|\gamma_{T0} + \theta_0|$, the angles between the players' velocity vectors and LOS_0, are close to $\pi/2$, an integral cost on u_M^2 and w_T^2 may be more appropriate. This representation enables a more straightforward tradeoff between the running cost and the terminal one, because the actual control effort is represented. It also eliminates the need to tune the weights in scenarios where the interception geometry changes throughout the engagement. Moreover, such a formulation ensures that the gains and the control commands u_M^* and w_T^* do not diverge when $\cos(\gamma_{M0} - \theta_0)$ or $\cos(\gamma_{T0} + \theta_0)$ approach zero.

I. Optimal Guidance Law

Similar to Eq. (13), we would like to minimize the following cost function:

$$J = \frac{a}{2}x_1^2(t_f) + \frac{b}{2}[x_4(t_f) - x_4^c]^2 + \frac{1}{2}\int_0^{t_f} u_M^2\,\mathrm{d}t \tag{A1}$$

By multiplying both sides of the cost function of Eq. (A1) by k_M^2, where $k_M = \cos(\gamma_{M0} - \theta_0)$, we get

$$J' = Jk_M^2 = \frac{a'}{2}x_1^2(t_f) + \frac{b'}{2}[x_4(t_f) - x_4^c]^2 + \frac{1}{2}\int_0^{t_f} u^2\,\mathrm{d}t;$$
$$a' \equiv ak_M^2, \qquad b' \equiv bk_M^2 \tag{A2}$$

Minimizing Eq. (A1) is equivalent to minimizing Eq. (A2), because the cost function was only multiplied by a constant. Furthermore, Eq. (A2) precisely equals Eq. (13) with weights a and b replaced by weights a' and b', respectively, and is constrained by the same dynamics. We can therefore expand the results presented in Sec. III to the required cost function by simply substituting a and b in Eqs. (22), (26), and (27) with a' and b', respectively. This results in the following guidance law:

$$u_M^*(t) = \frac{u^*(t)}{k_M} = \frac{\bar{N}_{\mathrm{ZEM}}}{t_{\mathrm{go}}^2}Z_1(t) + \bar{N}_{\mathrm{ZEAE}}\frac{V_M}{t_{\mathrm{go}}}[Z_2(t) - x_4^c] \tag{A3}$$

where

$$\bar{N}_{\mathrm{ZEM}} = \frac{N_{\mathrm{ZEM}}(a', b')}{k_M}, \qquad \bar{N}_{\mathrm{ZEAE}} = N_{\mathrm{ZEAE}}(a', b') \tag{A4}$$

and $N_{\mathrm{ZEM}}(a', b')$, $N_{\mathrm{ZEAE}}(a', b')$ are the navigation gains of Eq. (26) with a and b substituted with ak_M^2 and bk_M^2, respectively. For $k_M \to 0$, these navigation gains degenerate to

$$\bar{N}_{\mathrm{ZEM}}(k_M \to 0) = ak_M t_{\mathrm{go}}^3\left[1 - \frac{bt_{\mathrm{go}}}{2(bt_{\mathrm{go}} + V_M^2)}\right],$$
$$\bar{N}_{\mathrm{ZEAE}}(k_M \to 0) = \frac{-bt_{\mathrm{go}}}{bt_{\mathrm{go}} + V_M^2} \tag{A5}$$

Therefore, the navigation gains of u_M^* are bounded for $\cos(\gamma_{M0} - \theta_0) \to 0$.

II. Linear Quadratic Differential Games Guidance Law

Similar to the OGL formulation, we would like to expand the LQDG guidance law results to the following cost function:

$$J = \frac{a}{2}x_1^2(t_f) + \frac{b}{2}[x_4(t_f) - x_4^c]^2 + \frac{1}{2}\int_0^{t_f}(u_M^2 - \eta^2 w_T^2)\,\mathrm{d}t \tag{A6}$$

Using the same methodology with $k_T = \cos(\gamma_{T0} + \theta_0)$, we obtain

$$J' = Jk_M^2 = \frac{a'}{2}x_1^2(t_f) + \frac{b'}{2}[x_4(t_f) - x_4^c]^2 + \frac{1}{2}\int_0^{t_f}(u^2 - \eta'^2 w^2)\,\mathrm{d}t;$$
$$\eta' \equiv \frac{\eta k_M}{k_T} \tag{A7}$$

We can therefore expand the results presented in Sec. IV to the required cost function by substituting a, b, and η in Eqs. (45) and (48–50) with a', b', and η', respectively. This results in the following guidance law:

$$u_M^*(t) = \frac{u^*(t)}{k_M} = \frac{\bar{N}^u_{\mathrm{ZEM}}}{t_{\mathrm{go}}^2}Z_1(t) + \bar{N}^u_{\mathrm{ZEAE}}\frac{V_M}{t_{\mathrm{go}}}[Z_2(t) - x_4^c] \tag{A8a}$$

$$w_T^*(t) = \frac{w^*(t)}{k_T} = \frac{\bar{N}^w_{\mathrm{ZEM}}}{t_{\mathrm{go}}^2}Z_1(t) + \bar{N}^w_{\mathrm{ZEAE}}\frac{V_M}{t_{\mathrm{go}}}[Z_2(t) - x_4^c] \tag{A8b}$$

where

$$\bar{N}^u_{\mathrm{ZEM}} = \frac{N^u_{\mathrm{ZEM}}(a', b', \eta')}{k_M}, \qquad \bar{N}^u_{\mathrm{ZEAE}} = N^u_{\mathrm{ZEAE}}(a', b', \eta') \tag{A9a}$$

$$\bar{N}^w_{\mathrm{ZEM}} = \frac{N^w_{\mathrm{ZEM}}(a', b', \eta')}{k_T}, \qquad \bar{N}^w_{\mathrm{ZEAE}} = \frac{k_M}{k_T}N^w_{\mathrm{ZEAE}}(a', b', \eta') \tag{A9b}$$

$N^u_{\mathrm{ZEM}}(a', b', \eta')$, $N^u_{\mathrm{ZEAE}}(a', b', \eta')$, $N^w_{\mathrm{ZEM}}(a', b', \eta')$, and $N^w_{\mathrm{ZEAE}}(a', b', \eta')$ are the navigation gains of Eqs. (48) substituted with ak_M^2, bk_M^2, and $\eta k_M/k_T$, respectively.

For $k_M \to 0$, the missile's navigation gains degenerate to

$$\begin{aligned} \bar{N}^{\,u}_{\mathrm{ZEM}}(k_M \to 0) &= -\frac{3abt_{\mathrm{go}}^4 k_T}{2V_T \bar{K}_1 (3\eta^2 - ak_T^2 t_{\mathrm{go}}^3)}, \\ \bar{N}^u_{\mathrm{ZEAE}}(k_M \to 0) &= -\frac{bt_{\mathrm{go}}}{\bar{K}_1 V_M^2} \end{aligned} \tag{A10}$$

where

$$\bar{K}_1 = 1 - bt_{\mathrm{go}}\left(\frac{V_M^2 - V_T^2\eta^2}{V_M^2 V_T^2 \eta^2}\right) - \frac{3abt_{\mathrm{go}}^4 k_T^2}{4V_T^2(3\eta^2 - ak_T^2 t_{\mathrm{go}}^3)} \tag{A11}$$

Therefore, the navigation gains of u_M^* are bounded for $\cos(\gamma_{M0} - \theta_0) \to 0$. Similar results can be obtained for the target, showing that the navigation gains of w_T^* are bounded for $\cos(\gamma_{T0} + \theta_0) \to 0$.

Acknowledgment

This work was supported in part by a Horev Fellowship through the Taub Foundation.

References

[1] Kim, M., and Grider, K. V., "Terminal Guidance for Impact Attitude Angle Constrained Flight Trajectories," *IEEE Transactions on Aerospace and Electronic Systems*, Vol. AES-9, No. 6, 1973, pp. 852–859. doi:10.1109/TAES.1973.309659

[2] Ryoo, C. K., Cho, H., and Tahk, M. J., "Closed-Form Solutions of Optimal Guidance with Terminal Impact Angle Constraint," *Proceedings of the IEEE Conference on Control Applications*, Inst. of Electrical and Electronics Engineers, New York, 2003, pp. 504–509.

[3] Ryoo, C. K., Cho, H., and Tahk, M. J., "Optimal Guidance Laws with Terminal Impact Angle Constraint," *Journal of Guidance, Control, and Dynamics*, Vol. 28, No. 4, 2005, pp. 724–732. doi:10.2514/1.8392

[4] Ryoo, C. K., Cho, H., and Tahk, M. J., "Time-to-Go Weighted Optimal Guidance With Impact Angle Constraints," *IEEE Transactions on Control System Technology: A Publication of the IEEE Control Systems Society*, Vol. 14, No. 3, 2006, pp. 483–492. doi:10.1109/TCST.2006.872525

[5] Song, T. L., Shin, S. J., and Cho, H., "Impact Angle Control for Planer Engagements," *IEEE Transactions on Aerospace and Electronic Systems*, Vol. 35, No. 4, 1999, pp. 1439–1444. doi:10.1109/7.805460

[6] Kim, B. S., Lee, J. G., and Han, H. S., "Biased PNG Law for Impact with Angular Constraint," *IEEE Transactions on Aerospace and Electronic Systems*, Vol. 34, No. 1, 1998, pp. 277–288. doi:10.1109/7.640285

[7] Idan, M., Golan, O., and Guelman, M., "Optimal Planar Interception with Terminal Constraints," *Journal of Guidance, Control, and Dynamics*, Vol. 18, No. 6, 1995, pp. 1273–1279. doi:10.2514/3.21541

[8] Bryson, E. A., and Ho, C. Y., *Applied Optimal Control*, Blaisdell, Waltham, MA, 1969, pp. 154–155, 282–289.

[9] Ben-Asher, J. Z., and Yaesh, I., *Advances in Missile Guidance Theory*, Vol. 180, Progress in Astronautics and Aeronautics, AIAA, Reston, VA, 1998, pp. 25–90.

[10] Shima, T., Idan, M., and Golan, O., "Sliding-Mode Control for Integrated Missile Autopilot Guidance," *Journal of Guidance, Control, and Dynamics*, Vol. 29, No. 2, 2006, pp. 250–260. doi:10.2514/1.14951

[11] Friedland, B., *Advanced Control System Design*, Prentice–Hall, Upper Saddle River, NJ, 1996, pp. 110–112.

[12] Zarchan, P., *Tactical and Strategic Missile Guidance*, Vol. 157, Progress in Astronautics and Aeronautics, AIAA, Washington, D.C., 1994, pp. 161–180.

[13] Garber, V., "Optimum Intercept Laws for Accelerating Targets," *AIAA Journal*, Vol. 6, No. 11, 1968, pp. 2196–2198. doi:10.2514/3.4962